# Rigid Fused Oligoporphyrins as Potential Versatile Molecular Wires. 2. B3LYP and SCF Calculated Geometric and Electronic Properties of 98 Oligoporphyrin and Related Molecules

**Jeffrey R. Reimers,*,† Lachlan E. Hall,† Maxwell J. Crossley,† and Noel. S. Hush†,‡**

*School of Chemistry and Department of Biochemistry, The University of Sydney, Sydney, NSW 2006, Australia*

*Received: June 16, 1998; In Final Form: December 7, 1998*

Over 100 oligoporphyrin (porphyrin molecules fused to each other through rigid acene-type bridges) molecules have now been synthesized, their long rigid $\pi$-bonded structures making them very suitable as molecular wires while their synthetic flexibility offers the possibility of tailoring their structural and electronic properties to match specific needs. To examine their basic operational principles and to explore synthetic possibilities, we optimize the geometry of 85 oligoporphyrin and related molecules including porphyrin dimers and trimers using the accurate B3LYP density-functional technique. Also, a scheme is developed by which accurate geometries of oligoporphyrins of arbitrary size can be estimated, and this is applied to determine the geometries of a further 13 porphyrin trimers and tetramers. At these geometries we analyze SCF orbital properties in order to determine the superexchange electronic couplings within the oligoporphyrins. Couplings are monitored for bridge-length dependence and interpreted in terms of a detailed description involving bridge−porphyrin orbital resonances, as well as in terms of a simpler picture in which $\pi$-electron delocalization is seen as a prerequisite for strong intramolecular coupling. Variations of the coupling with the nature of the bridge (e.g., naphthalene, anthracene, free-base or protonated 1,4,5,8-tetraazaanthracene, tetracene, pyrene, coronene, biphenylene, dicyclobuta[*a*,*d*]benzene, dicyclobuta[*b*,*g*]naphthalene, dicyclobuta[*b*,*h*]biphenylene, and bridges additionally fused to porphyrin meso positions) and porphyrin (e.g., porphyrin or bacteriochlorin, $\beta$-substituents such as methoxy and cyano, Mg, Zn, $Ru(CO)_2$, and free-base porphyrins) units are considered, and the physical origin of quinonoid switching is determined. Terminal "alligator clips" such as fused phenanthroline, here complexed with $Cu^{I}Cl_2$, are also considered.

## 1. Introduction

Fused rigid oligoporphyrins have many natural advantages[1,2] in potential applications as *molecular wires*,[3−9] molecules which can communicate electronic coupling and/or transfer electronic charge over macroscopically large distances, distances sufficiently large to span biological membranes and nanoelectrode gaps. These molecules can be thought of as comprised of various basic building blocks, chemically combined to produce the desired structure and function. Building blocks which to date have been synthesized[1,10−13] into oligoporphyrins include, of course, the basic porphyrin unit itself, inter-porphyrin bridge units such as 1,4,5,8-tetraazaanthracene (TAA) and its derivatives, and end groups such as phenanthrolines and thiophenes to serve as molecular "alligator clips",[12,14] connecting wires to the outside world. To date,[13] over 100 oligoporphyrins have been synthesized in our laboratories, including linear porphyrin tetramers and octamers having end to end spans of ca. 56 Å and ca. 118 Å, respectively. In principle, it is straightforward to produce longer chains than this as the synthetic strategy allows for doubling of the length with each step, and a large range of molecules with nonlinear topologies have also been made.

In part 1 of this series,[15] we considered TAA-bridged oligoporphyrins and showed that, at the simplest level, electronic properties are controlled by the degree of $\pi$ delocalization. Areas within the molecules in which the $\pi$-system forms discrete single and double bonds localize the $\pi$-electron wave functions either inside or outside of these regions, effectively insulating electrons on either side from each other, while delocalized regions support long-distance electronic communication. This simple idea may become a key design principle in molecular wire technology and has already been exploited with the synthesis of chemically controllable oligoporphyrin molecular switches:[13] in these, the central anthracene ring is made to be quinonoidal, with conversion of the quinonoid (or quinonoid dioxime) forms to the corresponding hydroquinone effectively converting a $\pi$-localized ring to a delocalized one and hence greatly enhancing the through-bridge coupling. Optical switches of this type are also possible.[16]

As calculated $\pi$ electron distributions are sensitive to the details of the geometries at which they are evaluated, in quantitative studies it is essential to use the best-possible estimate of the geometry. Not only is it important to correctly describe gross features such as porphyrin inner-hydrogen tautomerization, but also it is important to describe subtle features such as $\beta-\beta'$ pyrrole bond length variations. In part 1 we used what was then thought to be the best method available for determining these properties, the semiempirical PM3 method. While subsequent comparison with extensive ab initio MP2 calculations for free-base porphyrin[17] suggests that PM3 provides an adequate description of the relative energies of different tautomers, it is clear that PM3 geometries could be improved upon, especially for structures of low point-group symmetry.

* Corresponding author.
† School of Chemistry.
‡ Department of Biochemistry.

10.1021/jp982650j CCC: $18.00 
Published on Web 05/18/1999

Indeed, historically, accurate computation of the properties of porphyrin compounds has been quite difficult. Both ab initio and semiempirical self-consistent field (SCF) techniques fail to correctly balance the $\sigma$ and $\pi$ forces acting within porphyrins and consequently predict, incorrectly,[15] either that the molecule distorts from $D_{2h}$ symmetry to $C_{2v}$ (spin-restricted wave function) or that the molecule is a triplet biradical (spin-unrestricted wave function). In recent years, this difficulty has been overcome, with the correct high-symmetry geometry and singlet electronic structure obtained when electron correlation is taken into account using, e.g.,[18,19] local density functional (LDF), second-order Møller−Plesset perturbation (MP2), or higher levels of theory. Density functional techniques have now become feasible for extended porphyrin systems, promising reliable evaluation of the properties of these systems.

Here we employ the sophisticated B3LYP density-functional method with a 3-21G basis set via the GAUSSIAN-94 program package[20] to evaluate the geometry and electronic structure of oligoporphyrins. While this basis set is relatively small, it has been shown[21,22] to be adequate for many of our needs. We investigated this further through the evaluation of a variety of properties of free base porphyrin **85**. First and most important, geometry optimization predicts, correctly, a structure of $D_{2h}$ symmetry; the optimized coordinates are provided in the Supporting Information. Contrary to solution of the Hartree−Fock equation for porphyrin, the obtained solution of the Kohn−Sham equations is stable.[18,23] The root-mean-square deviation of the calculated bond lengths from the observed X-ray values[24] is 0.011 Å, less than the deviations of 0.014 Å calculated using the LDF and PM3 methods, 0.017 Å calculated using MP2, and 0.022 Å calculated using the AM1, MINDO, and MINDO/3 methods.[15] The structure was shown to be a local minimum by normal coordinate analysis. Good agreement is seen between the unscaled calculated frequencies and observed frequencies, the average and maximum errors being +42 and 177 $cm^{-1}$, respectively. Note that this analysis is based on Kozlowski et al.'s detailed assignment[25] of the relative ordering of normal modes of the same symmetry and, as several interchanges are found, these errors could actually be inflated.

We have also evaluated the first and second ionization potentials of free base porphyrin by direct evaluation of the energy of the porphyrin cations using spin-restricted B3LYP. The results of 6.87 eV ($a_u$) and 6.64 eV ($b_{1u}$) are close to the experimentally observed[26] values of 7.2 and 6.9 eV, of comparable accuracy to LDF[27] (7.44 eV ($a_u$) and 7.23 eV ($b_{1u}$)) but apparently significantly better than SCF[21,22,27] (6.6 eV ($b_{1u}$) and 6.3 eV ($a_u$)). This result is important as the calculation of ionization energies and electron affinities quantify aspects of through-molecular conduction.

We employ B3LYP rather than LDF as LDF is known to fail for highly extended conjugated systems.[18,28,29] B3LYP offers the possibility of correction for this inadequacy. In calculations[30] of the superexchange couplings between finite-length polyene-bridged bis(ruthenium) complexes, we found that the calculated band gap narrowed beyond that of polyacetylene, as did the bond-length attenuation, and so this problem may remain. It is unclear what related effects are likely to occur for oligoporphyrins, however. Another possibly related aspect (not discussed in this paper) in which we find density functional calculations to be wanting is the evaluation of electronic spectral properties of porphyrins. We reproduce using TURBOMOLE-4[31] the time-dependent density-functional calculations of Bauernschmitt and Ahlrichs[32] which depict electronic transition energies close to those observed for porphyrin Q and B bands and verify that B3LYP/3-21G gives similar results. However, in all cases, we find that the transitions predicted to occur in the region of the B band actually have an alternate origin and in fact that the characteristically sharp and intense B bands appear smeared over a very large number of transitions.

The aims of this work are, in order of increasing importance, (1) to revise our scheme[15] for estimating the geometry of an arbitrary oligoporphyrin, (2) to calculate improved estimates of the inter-porphyrin coupling in known molecules, (3) to investigate the effects of subtle chemical changes on the electronic communication, and (4) to design oligoporphyrin systems with enhanced properties. In all, optimized structures for 85 oligoporphyrin and related molecules are evaluated using B3LYP with a 3-21G basis set via GAUSSIAN-94.[20] These molecules are listed later in Tables 1, 2, 4, and 5, and their structures, optimized coordinates, evaluated Mulliken charges, and total energies are given in full in the Supporting Information. Structures for a further 13 porphyrin trimers and tetramers are estimated, when required. At the broadest level all molecules studied are classified as $P_nB_mE_l$ where P is a porphyrin, B is a bridge unit, and E is an end group which replaces a terminal porphyrin. All B3LYP optimizations are performed assuming the maximum point-group symmetry. The different components used for P (substituted porphyrins, bacteriochlorin), B (benzene, naphthalene, anthracene, TAA, tetracene, dicyclobuta[*a*,*d*]benzene (DCB), biphenylene, dicyclobuta[*b*,*g*]naphthalene (DCN), dicyclobuta[*b*,*h*]biphenylene (DCP), pyrene, coronene), and E (thiophene, phenanthroline−$[CuCl]^-$) are shown in Figure 1. The process employed to connect the various P, B, and E units into a single molecule usually involves ring fusion along a single CC bond (for a porphyrin, this is a $C_\beta-C_\beta$ bond). For two bridges, named *f*-anthracene and *f*-coronene, additional CH units are added to fuse new rings between the bridge and porphyrin meso positions. The electronic structures of such $P_1B_1$ units are shown in Figure 2.

There are many observable molecular phenomena whose interpretation is most conveniently made by describing the molecule as a "molecular wire". Most literally, this is demonstrated in some new experiments which measure the current passing between two electrodes connected via a single molecule.[3−9] More traditionally, this is demonstrated by thermally or spectroscopically initiated intramolecular electron or hole conduction processes. Proper theoretical treatments should be tuned for the particular property of interest, but a good overall impression of the molecular aspects of both[9] electrode and intramolecular conduction processes can be obtained by considering superexchange properties of the frontier orbitals of the different parts of the molecules involved. This is the approach taken herein. Specifically, for the case of hole-transport through symmetrical dimers of the class $P_2B_1$, the conceptually most simple approach is to assume an effective two-level model in which one porphyrin is thought to be a hole "donor" with the other as a hole "acceptor". Superexchange conduction is then controlled[33] by an inter-porphyrin electronic coupling $J$ whose magnitude is equal to half of the energy difference between the first and second ionization potentials of the dimer. For a given molecule these ionization energies can be explicitly evaluated using either SCF or B3LYP total energies, and results obtained using these two approaches for oligoporphyrins agree quite well.[13] Ionization-energy calculations are expensive and difficult, but reliable SCF results may be obtained with ease through the application of Koopmans' theorem; this allows $J$ to be determined simply from the differences in the energies of paired molecular orbitals, and we

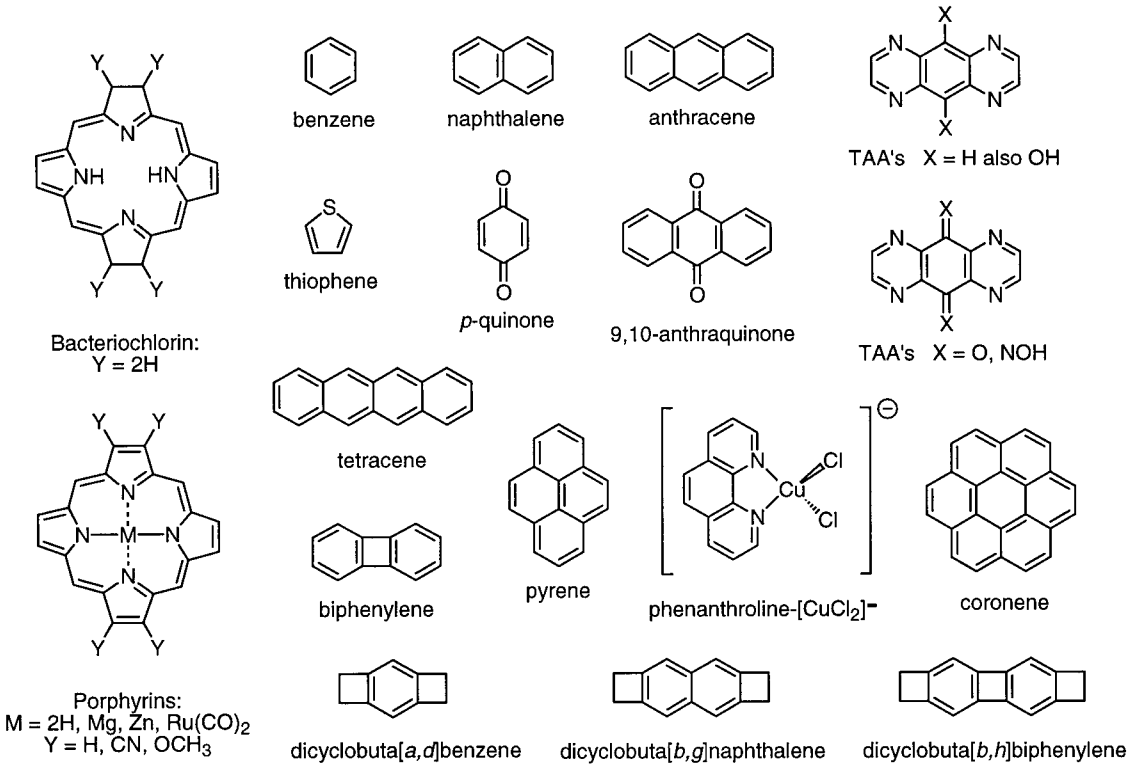


**Figure 1.** Component molecules subsequently fused to form oligoporphyrins.

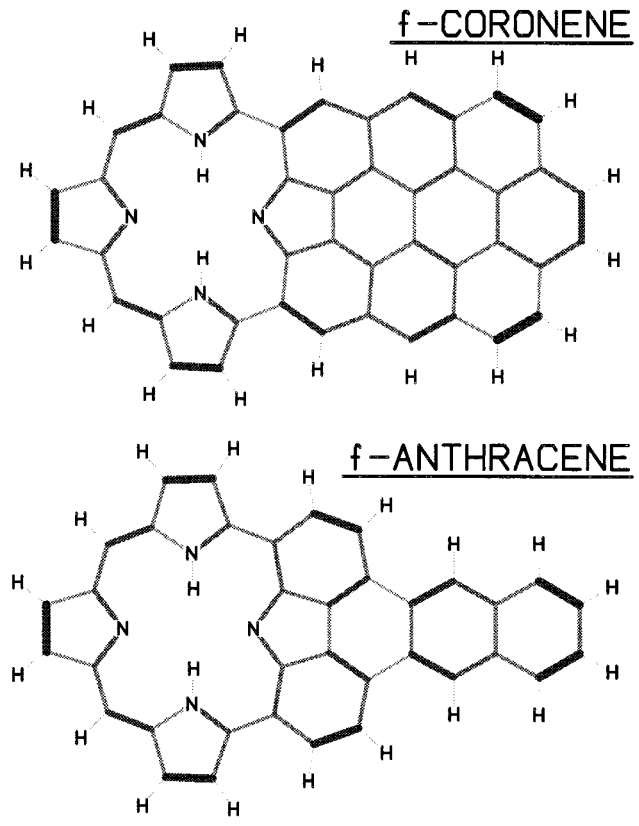


**Figure 2.** B3LYP/3-21G optimized structures and SCF/3-21G $\pi$ atomic bond orders for $P_1B_1$ complexes with B = *f*-anthracene (**64**) and *f*-coronene (**65**) in which the additional rings are fused between the anthracene and coronene bridges to the porphyrin meso positions, respectively. Full $\pi$ bonds are indicated by thick black lines, while weak $\pi$ bonds are depicted by thin, faint lines; see Figure 7.

adopt this approach. It requires, however, that calculated molecular orbitals be described in terms of symmetry-adapted linear combinations of orbitals localized on each individual P, B, or E fragment. In most cases this process is straightforward, but if orbitals on adjacent fragments lie very close in energy, resonance will occur making partitioning difficult. As the coupling between fragments increases, so does the probability of resonance.

At resonance, the kinetics of transport processes through molecules is poorly represented using effective two-level models.[33,34] Quantitative analysis of such resonances is not the object of this work, however, and it is sufficient for our purposes here to flag the occurrence of resonance through the evaluation of very large effective two-level couplings *J*. Some of the compounds which we consider are either chelated ruthenium(II) porphyrins or attached copper(I) complexes; for these it is possible to study not only couplings between porphyrin-based orbitals but also couplings between the metal $d_\pi$ orbitals. Here we investigate the relatively straightforward problem of coupling between the porphyrin-based orbitals only. A thorough analysis of hole-transfer kinetics through the resonance region for intermetallic coupling in metallooligoporphyrins *without* invocation of an effective two-level model has been performed and the results are described elsewhere.[2] Similar calculations have also been performed for bis(ruthenium polyene) complexes[30] for which detailed experimental data are available.

Our calculations in part 1 of this series[15] used PM3 to determine geometries and CNDO/S to determine molecular orbital energies and thus inter-porphyrin couplings. In comparison of calculated electronic couplings evaluated at PM3 and B3LYP geometries[13] for bis(porphyrins) containing quinonoid, hydroquinonoid, and quinonoid dioxime bridges, it is clear that use of PM3 geometries produces qualitatively descriptive results, but quantitatively calculated couplings can vary by a factor of 2. For the same systems we also have recently found that, compared to ab initio SCF and B3LYP results, these CNDO/S energies are only accurate to within a factor of 2. Hence, while the original methods are capable of reproducing gross effects (such as quinonoid−hydroquinonoid switching), they are inad-

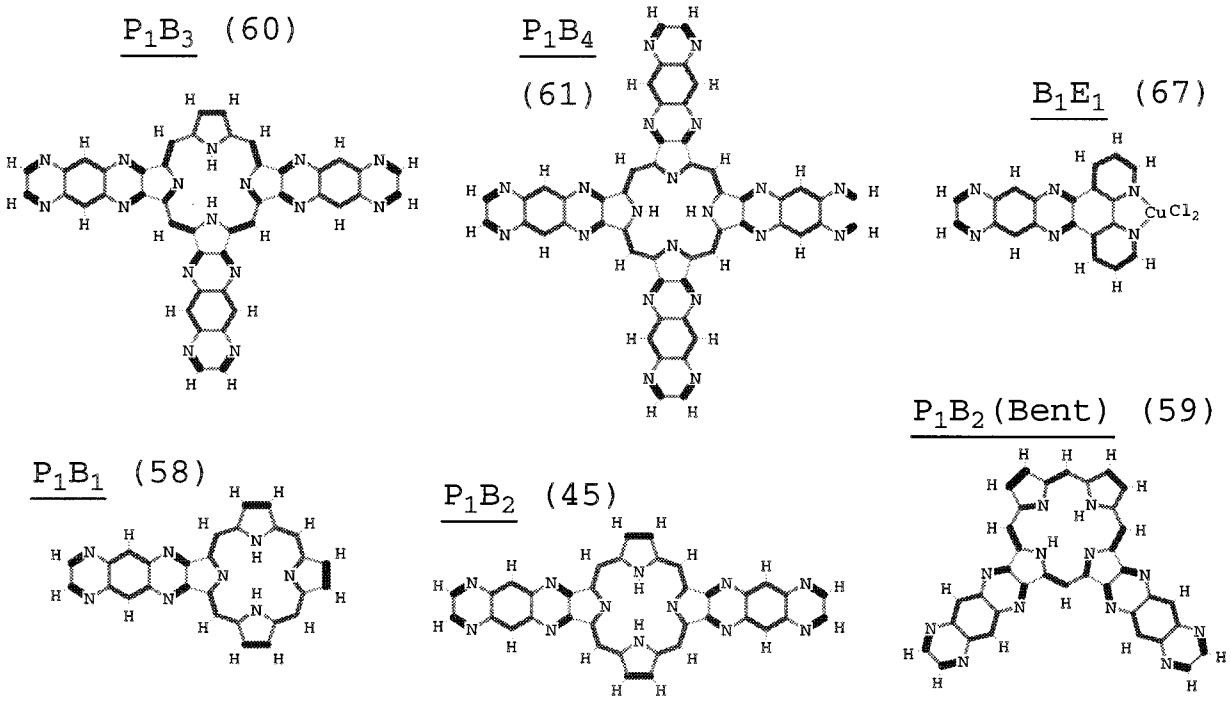


**Figure 3.** SCF/3-21G atomic bond orders at the B3LYP/3-21G structures for the six standard building blocks used for describing the structure of an arbitrary oligoporphyrin. Full $\pi$ bonds are indicated by thick black lines, while weak $\pi$ bonds are depicted by thin, faint lines.

equate in describing more subtly chemical variations, variations which are relevant to the design of practical functioning devices. The method employed herein, determining couplings by considering SCF orbital energies at B3LYP optimized (or estimated) geometries, is expected to be robust and reliable, and it is now feasible to examine of order 100 oligoporphyrins in a computational study via this approach. In our preliminary study[13] we showed that results obtained using this approach can (at least) qualitatively describe observed properties of oligoporphyrins. Further, elsewhere[30] we have shown that they can quantitatively describe the observed intermetallic coupling in bis(ruthenium) complexes.

## 2. Technical Innovations

SCF and B3LYP calculations are performed using Gaussian-94.[20] However, for the oligoporphyrins comprising bis Ru(II) (low-spin $d^6$) or Cu(I) (closed-shell $d^{10}$) complexes, standard means of converging the Fock or Kohn−Sham loops either fail or become prohibitively expensive due to the large molecular size and the dense manifold of low-energy electronic states available (within ca. 1 part in $10^5$ of the total energy of the ground state). To complete these calculations, we developed a scheme for the accurate prediction of the molecular orbitals of a molecule on the basis of those already obtained for smaller fragments. This involves the overlaying of fragment molecules, deletion of atoms not present in the target molecule, and the averaging of either the individually orthogonalized Fock/Kohn−Sham or density matrix elements between all of the remaining atoms. The resulting matrix for the target molecule is then diagonalized and back-transformed using the full molecular overlap matrix to produce initial orbitals for Gaussian-94. Rapid convergence of the subsequent calculations was then obtained.

## 3. Geometries of Oligoporphyrins

To date, the most frequently used bridge molecule in oligoporphyrins has been 1,4,5,8-tetraazaanthracene (TAA). Our previous PM3 calculations[15] showed that the skeletal geometry of one of these oligoporphyrins is controlled by the pattern of bridge attachment to the four possible attachment sites and by inner hydrogen tautomerization; the results obtained are expected to typify those for a large variety of different bridging materials. As the PM3 results for the most stable tautomers are expected to be reliable,[17] we consider only these structures herein. An important observation made was that the presence or absence of another porphyrin at the end of an attached bridge did not have a significant geometrical influence. Assuming this, the geometry of an arbitrary $P_nB_mE_l$ oligoporphyrin can be estimated by combining the structures of six basic building blocks: $B_1E_1$, $P_1B_1$, linear $P_1B_2$, bent $P_1B_2$, $P_1B_3$, and $P_1B_4$, the structures of which are shown in Figure 3 for an unsubstituted porphyrin or phenanthroline−$[CuCl_2]^-$ end group fused to TAA bridges.

The method used to construct the geometry of an arbitrary oligoporphyrin from those of the building-block porphyrins involves cutting each bridge unit in half (for TAA, this occurs along the plane containing its $C_9$ and $C_{10}$ atoms); the tail sections are discarded, and complex molecules are assembled by splicing, averaging the coordinates of the duplicated (nominally C and H) atoms at the splice. This process is indicated in Figure 4 for the construction of a $P_3B_2$ (**2**) from two $P_1B_1$'s (**58**) and one $P_1B_2$ (**45**) using P = free-base porphyrin and B = TAA. Accuracy is gauged by comparing the bond lengths obtained from this construction with those obtained by fully optimizing the geometry, and results obtained for a variety of oligoporphyrins are summarized in Table 1. The results indicate that for oligoporphyrins bridged by TAA this construction scheme works extremely well, the largest error recorded in any one bond length for the five molecules considered being just 0.003 Å. For DCB and *f*-coronene bridges, this error increases to 0.018 and 0.037 Å, respectively, but the root-mean square errors remain less than 0.004 Å. As we shall see later, these bridges strongly perturb the electronic structure of the porphyrin, giving rise to significantly enhanced inter-porphyrin coupling; for these exceptional cases, simplistic geometric schemes are less appropriate.

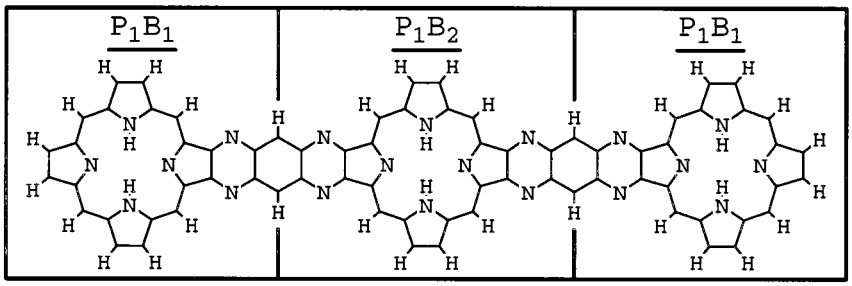


**Figure 4.** Construction method used to construct $P_3B_2$ **2** through the combination of the individually optimized geometries for two $P_1B_1$ units **58** and one $P_1B_2$ unit **45**. The coordinates of border atoms are averaged; see text.

**TABLE 1: Root-Mean-Square (Rms) and Maximum Errors in the Bond Lengths between Estimated Geometries (See Text) of Linear Oligoporphyrins and the Corresponding B3LYP/3-21G Optimized Structures**

| | | | bridge | | | error/Å | |
|---|---|---|---|---|---|---|---|
| no. | class | porphyrin inner ring | type | sub-stituent | made from | rms | max |
| **1** | $P_2B_1$ | 2H | TAA | H | **58** | 0.0003 | 0.0008 |
| **2** | $P_3B_2$ | 2H | TAA | H | **58**, **45** | 0.0003 | 0.0007 |
| **3** | $P_2B_1$ | 2H | TAA | O | **62** | 0.0005 | 0.0018 |
| **4** | $P_2B_1$ | $Ru(CO)_2$ | TAA | H | **63** | 0.0002 | 0.0004 |
| **5** | $B_1E_2$ | | TAA | H | **67** | 0.0012 | 0.0027 |
| **6** | $P_2B_3$ | 2H | DCB | H | **50** | 0.0039 | 0.018 |
| **7** | $P_3B_2$ | 2H | DCB | H | **35, 51** | 0.0033 | 0.016 |
| **8** | $P_2B_1$ | 2H | *f*-coronene | | **65** | 0.0060 | 0.025 |
| **9** | $P_3B_2$ | 2H | *f*-coronene | | **43**, **51** | 0.0102 | 0.037 |

[a] P, porphyrin; B, bridge; E, phenanthroline−$[CuCl_2]^-$ end group; TAA, 1,4,5,8-tetraazaanthracene; DCB, dicyclobuta[*a*,*d*]benzene; *f*-coronene, coronene with extra CH's to fuse additional rings to the porphyrin meso positions (see Figure 2).

### 4. Effects of Chemical Variations

One of the advantages of the use of porphyrin-based molecular wires is the considerable synthetic variability which may be built into the design. The porphyrins may be substituted at both the $\beta$ and meso positions, undergo inner-ring metal chelation, and can be converted into chlorins, bacteriochlorins, etc.; synthetic variations on the bridging material are also possible. Here, we consider in detail the effects of five easily achievable synthetic variations to the structure and function of the oligoporphyrins $P_2B_1$ and $P_1B_2$: (i) porphyrin $\beta$ substitution with cyano or methoxy groups as well as $\beta$ hydrogenation to form bacteriochlorins (bacteriochlorin itself is **84**); (ii) chelation of the divalent species Mg, Zn, and $Ru(CO)_2$ inside the porphyrin rings; (iii) use of quinonoid linkages within bridges (bridge substitution); (iv) use of different bridges (bridge type), and (v) protonation of bridge azine nitrogens (bridge protonation).

**4.1. Variations i−iv of $P_2B_1$.** A total of 38 different molecules of class $P_2B_1$ have been considered, derived by combining variations i−iv in different ways. For these, calculated couplings between localized porphyrin second-highest-occupied fragment molecular orbital (SHOMO), highest-occupied fragment molecular orbital (HOMO), lowest-unoccupied fragment molecular orbital (LUMO), and second-lowest-unoccupied fragment molecular orbital (SLUMO) levels are given in Table 2; the magnitude $|J|$ of these couplings is evaluated as half of the SCF energy splitting between the symmetric and antisymmetric linear combinations of the localized porphyrin orbitals, while the sign of the coupling is determined by the relative ordering: we take positive coupling to dictate that the highest-lying molecular orbital is symmetric with respect to the plane of symmetry which bisects the bridge. Because the porphyrin HOMO/SHOMO and LUMO/SLUMO pairs have only small energy separations, no unique identification is possible. Indeed, in metalloporphyrins of $D_{4h}$ symmetry, the LUMO and SLUMO are degenerate, and we find that their order readily interchanges in oligoporphyrins, as indicated in Table 2. As mentioned in the Introduction, for free-base porphyrin, the HOMO and SHOMO levels are only slightly split in energy and the issue as to the actual symmetry of the HOMO level is not yet fully resolved. We define the localized SHOMO, HOMO, LUMO, and SLUMO orbitals on the basis of their SCF ordering in free-base porphyrin. To illustrate this, the four pairs of molecular orbitals calculated for **1** ($P_2B_1$ with B = TAA) are shown in Figure 5; note that, for this molecule, the SLUMO/LUMO order is opposite to that in free-base porphyrin. In this figure, nonzero coefficients on bridge sites indicates that significant interactions between porphyrin orbitals and bridge orbitals occur.

To aid in the interpretation of Table 2, the calculated SCF $\pi$ atomic bond orders for the oligoporphyrins **1**, **3**, **10**, **23**, **35**, and **43** are shown in Figure 6; similar results for the $P_1B_1$ oligoporphyrins **64** and **65** are also shown in Figure 2, while those for benzene (**69**) and *p*-quinone (**70**) are shown in Figure 7. Atomic bond orders[35] are used as they are uniquely defined for all molecules using all basis sets. They differ from older bond order definitions in that they are squares of off-diagonal density-matrix elements, with the result that the Hückel $\pi$ bond order for benzene is (the more intuitive value of) $^4/_9$ rather than $^2/_3$. In these figures, double bonds are represented as thick, dark lines while single bonds are represented as thin, faint lines; this is illustrated most clearly in Figure 7 where benzene is compared directly to *p*-quinone.

The results shown in Table 2 indicate that the SHOMO, HOMO, LUMO, and SLUMO orbital interactions differ significantly in magnitude and are modulated differently by the various chemical changes. Coupling through SHOMO orbitals, which have large coefficients on the pyrrole nitrogens in metalloporphyrins, is usually quite small with $|J|$ ]averaging around 17 meV. This coupling typically decreases by a factor of 4 when the bridge is converted from benzenoid form (bridge substituent H or OH) to quinonoid form (bridge substituent O or NOH). To highlight this effect, the average magnitudes of the coupling for the 12 oligoporphyrins listed in Table 2 with both benzenoid and quinonoid forms, as well as the average attenuations in this coupling resulting from benzenoid to quinonoid conversion, are shown in Table 3.

Large interactions between terminal SHOMO orbitals are found, however, when the bridge is *f*-coronene. In this case, the bridge levels fall into resonance with porphyrin levels. The electronic structure of the porphyrins is seriously disturbed by this bridge with the molecular orbitals not easily recognizable as linear combinations of porphyrin orbitals. Indeed, the $\pi$ bond orders shown for this molecule in Figure 6 suggest that it could

**TABLE 2: Calculated Couplings between the Porphyrin SHOMO, HOMO, LUMO, and SLUMO Levels in Substituted Symmetrical Dimers $P_2B_1$**

| | porphyrin | | bridge | | coupling/meV | | | |
|---|---|---|---|---|---|---|---|---|
| no. | $\beta$ substituent | inner ring | type[f] | substituent | SHOMO | HOMO | LUMO | SLUMO |
| **1** | H | 2H | TAA | H | −3 | 119 | 159[c] | −126 |
| **10** | H | 2H | anthracene | H | −2 | 196 | 194[c] | −54 |
| **3** | H | 2H | TAA | O | 0 | −3 | −178 | −31 |
| **11** | H | 2H | anthracene | O | 0 | −19 | −207 | −13 |
| **12** | H | 2H | TAA | OH[b] | −2 | 191 | 189[c] | −103 |
| **13** | H | 2H | TAA | NOH[b] | 2 | 18 | −33 | −24 |
| **14** | H | Mg | TAA | H | −28 | 105 | 184[c] | −229 |
| **15** | H | Mg | anthracene | H | −26 | 174 | 217[c] | −116 |
| **16** | H | Mg | TAA | O | −6 | −9 | −224 | −65 |
| **17** | H | Mg | anthracene | O | −7 | −20 | −254 | −29 |
| **18** | H | Zn | TAA | H | −28 | 107 | 182[c] | −227 |
| **29** | H | Zn | anthracene | H | −30 | 178 | 218[c] | −131 |
| **20** | H | Zn | TAA | O | −7 | −8 | −229 | −65 |
| **21** | H | Zn | anthracene | O | −8 | −21 | −260 | −33 |
| **4** | H | $Ru(CO)_2$ | TAA | H | −19 | 114 | 178[c] | −201 |
| **22** | H | $Ru(CO)_2$ | TAA | O | −5 | −7 | −226 | −46 |
| **23** | 2H | 2H | TAA | H | −75 | 57 | −291[d] | 487 |
| **24** | 2H | 2H | TAA | O | −17 | −17 | −238 | 532 |
| **25** | 2H[a] | 2H | TAA | H | −2 | 116 | 177 | −242 |
| **26** | 2H[a] | 2H | anthracene | H | −3 | 106 | 277 | 203 |
| **27** | 2H[a] | 2H | TAA | O | 0 | −24 | −82 | 321 |
| **28** | 2H[a] | 2H | anthracene | O | 0 | −37 | −154 | 260 |
| **29** | CN | 2H | TAA | H | −2 | 137 | 138[c] | −31 |
| **30** | CN | 2H | TAA | O | 0 | −3 | −128[c] | −9 |
| **31** | $OCH_3$ | 2H | TAA | H | −2 | 132 | 143[c] | −149 |
| **32** | $OCH_3$ | 2H | TAA | O | 0 | −8 | −137 | −36 |
| **33** | H | 2H | naphthalene | H | 4 | −220 | −279 | 47 |
| **34** | H | 2H | tetracene | H | 1 | −190 | 82[c] | −136 |
| **35** | H | 2H | DCB | H | 8 | 385[e] | −701 | 184 |
| **36** | H | $Ru(CO)_2$ | DCB | H | 71 | 367[e] | −711 | 279 |
| **37** | H | 2H | biphenylene | H | −8 | −76 | −165 | −24 |
| **38** | H | 2H | DCN | H | −27 | −36[e] | −73 | 22 |
| **39** | H | 2H | DCP | H | −28 | −130[e] | 273 | 94 |
| **40** | H | 2H | pyrene | | 5 | 31 | 139 | 61 |
| **41** | H | 2H | coronene | | −5 | −120 | −162 | 7 |
| **42** | H | 2H | *f*-anthracene | H | −71 | 144 | 245[c] | −84 |
| **43** | H | 2H | *f*-coronene | | 805 | −35[e] | 107[c] | 192 |
| **44** | H | $Ru(CO)_2$ | *f*-coronene | | 770 | −101[e] | 222[c] | ? |

[a] Higher-energy form with the inner hydrogens along the short axis. [b] Lowest-energy conformer ($C_{2h}$ symmetry).[13] [c] SLUMO and LUMO reversed in energy compared to free-base porphyrin (LUMO has coefficient on the possibly protonated short-axis N's). [d] An unoccupied bridge orbital is lower in energy. [e] An occupied bridge orbital is higher in energy. [f] TAA, 1,4,5,8-tetraazaanthracene; DCB, dicyclobuta[*a*,*d*]benzene; DCN, dicyclobuta[*b*,*g*]naphthalene; DCP, dicyclobuta[*b*,*h*]biphenylene; *f*-anthracene and *f*-coronene, anthracene and coronene with extra CH's to fuse additional rings to the porphyrin meso positions, respectively (see Figure 2).

be described not as an oligoporphyrin but rather as a small piece of graphite with metal binding sites at the ends!

Calculated couplings between the HOMO levels typically range over 100 meV $< |J| <$ 200 meV for benzenoid bridges. As shown in Table 3, this coupling is attenuated on average by a factor of 15 after quinonoid conversion of the bridge. This effect parallels that described previously for the SHOMO levels and, the effects of accidental resonances notwithstanding, can most easily be understood by comparison of the $\pi$ atomic bond orders shown in Figure 6 for the benzenoid compound **1** (B = TAA) and its quinonoid derivative **3**. Strong end to end coupling through bonding orbitals arises when the intermediate bonds are all delocalized (ie., appear as a uniform gray in Figure 6 a la benzene in Figure 7). Quinonoid conversion results in the destruction of the delocalization through the central bridge ring, however, and this dramatically reduces the end to end coupling. This effect also explains most of the minor effects seen such as the stronger coupling for pure CH bridges such as anthracene (**10**) compared to aza-substituted bridges such as TAA (**1**); see Figure 6.

The quinonoid effect is expected to be very general in application. To test this we investigated the coupling between the sulfur lone pair orbitals in 1,3-bis(2-thienyl)benzene (**56**) and 2,6-bis(2-thienyl)-1,4-benzoquinone (**57**). In this fashion, a quinonoid switch could, as an example, be introduced into a polythiophene molecular wire. The effects are again significant, with the magnitude of the coupling between the thiophene HOMO (sulfur lone pair) orbitals decreasing by a factor of 4 when the quinonoid is produced. Superexchange-controlled electron-transfer rate constants are likely[13,33] to scale with the square of *J*, and hence, the quinonoid effect is calculated to reduce rates by in excess of 1 order of magnitude per linkage.

While oligoporphyrins such as **1** (B = TAA) and **10** (B = anthracene) shown in Figure 6 clearly have strong delocalization paths both within their porphyrin units and within their bridge units, delocalization is clearly restricted in the vicinity of the fused $C_\beta-C_\beta$ bonds. These bonds are nearly full single bonds, and they have the effect of forcing the adjacent $C_\alpha-C_\beta$ bonds to be single and the $C_\beta$−bridge bonds to be double. We examined ways in which this scenario could be changed by conversion of the porphyrins to bacteriochlorins and by changing the nature of the bridge.

Bacteriochlorin conversion was found to increase localization, however, with the calculated couplings for **23**−**28** decreasing

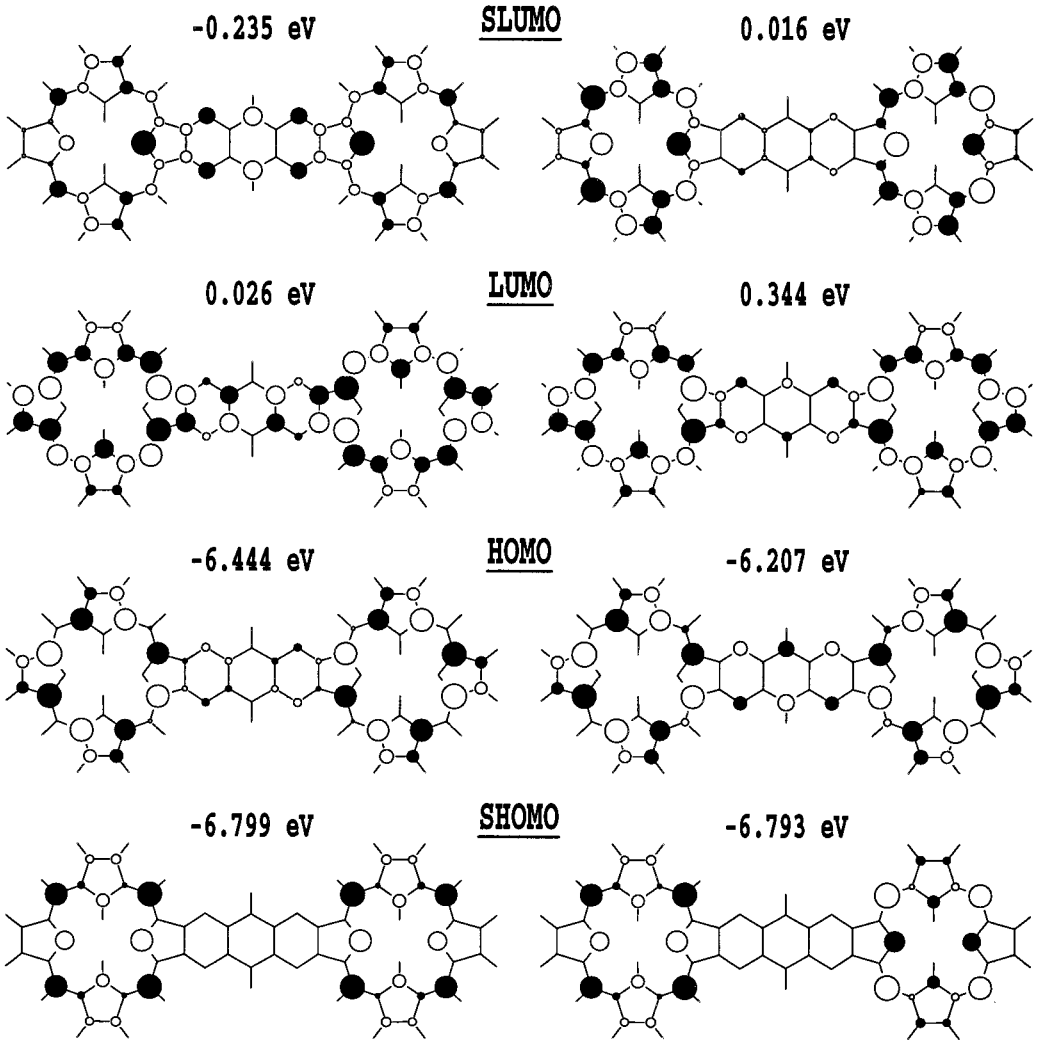


**Figure 5.** Four highest-lying occupied molecular orbitals and four lowest-lying unoccupied molecular orbitals and their energies for $P_2B_1$ **1** (evaluated SCF/3-21G at the B3LYP/3-21G geometry) analyzed in terms of pairs of localized porphyrin SHOMO, HOMO, LUMO, and SLUMO levels. The areas of the circles indicate the relative contribution of the orbital, if occupied, to the atomic Mulliken charge, while open and closed circles are used to indicate the sign of the wave function.

somewhat. There are two inner-hydrogen tautomers possible for bacteriochlorin-one with the hydrogens along the short axis (as for other oligoporphyrins), bound to the hydrogenated pyrroles, and one with the hydrogens along the long axis, bound to the fused pyrroles. At the B3LYP/3-21G level, the long-axis tautomer of $P_2B_1$, molecule **23**, is predicted to be more stable than its short-axis tautomer **25** by 23 kcal $mol^{-1}$. The location of the inner hydrogens has a profound effect on the electronic structure, however, with that for **25** (not shown) being quite similar to that for **3** (shown in Figure 6), quite distinct from that of **23** (shown in Figure 6).

To study the influence of the nature of the bridge, oligoporphyrins **33**−**44** were optimized using a variety of alternate bridges. In most cases delocalization was not significantly improved around the $C_\beta-C_\beta$ bond and was often lost within the bridge itself; results for B = DCB (**35**) and *f*-coronene (**43**) are shown in Figure 6. For the DCB bridge the HOMO coupling is very strong, but this arises not from increased delocalization but rather from an accidental resonance with a bridge orbital. Delocalization is significantly enhanced for the *f*-coronene bridge, but again it is the nature of the resonances with the bridge which control the end-to-end coupling. This delocalization does not occur for B = coronene (**41**) and hence does not arise because of the size or shape of the bridge, and it also does not occur for B = *f*-anthracene (**42**) and hence does not arise from the rings fused to the porphyrin meso positions. Clearly the delocalization, like the resonances generated, is a property of the whole system. The oligoporphyrins formed with the dicyclobuta-containing links (DCB, DCN, and DCP) as well as those containing *f*-coronene bridges all have occupied bridge orbitals of higher energy than the porphyrin HOMO levels, and thus, resonances are very likely. Hole transport properties will be dominated by the highest occupied molecular orbitals, and so these bridge orbitals become very important. The final conclusion is that, for the most efficient hole transport through oligoporphyrins, one would wish the bridge and oligoporphyrin highest-occupied levels to be of very similar energy, maximizing resonance effects.

Couplings between the porphyrin SLUMO levels quite resemble those between the porphyrin HOMO levels. SCF calculations, as indicated in Table 2, predict that these orbitals form the lowest unoccupied level for many $P_2B_1$ complexes, including the numerous B = TAA complexes such as **1**, and thus become the most important levels for electron transport. Quinonoid conversion (e.g., **3**, **13**) reduces the coupling by typically a factor of 3 but inverts the order of the molecular orbitals so that electron conduction would be controlled instead by the (much larger) inter-LUMO couplings. Thus, while

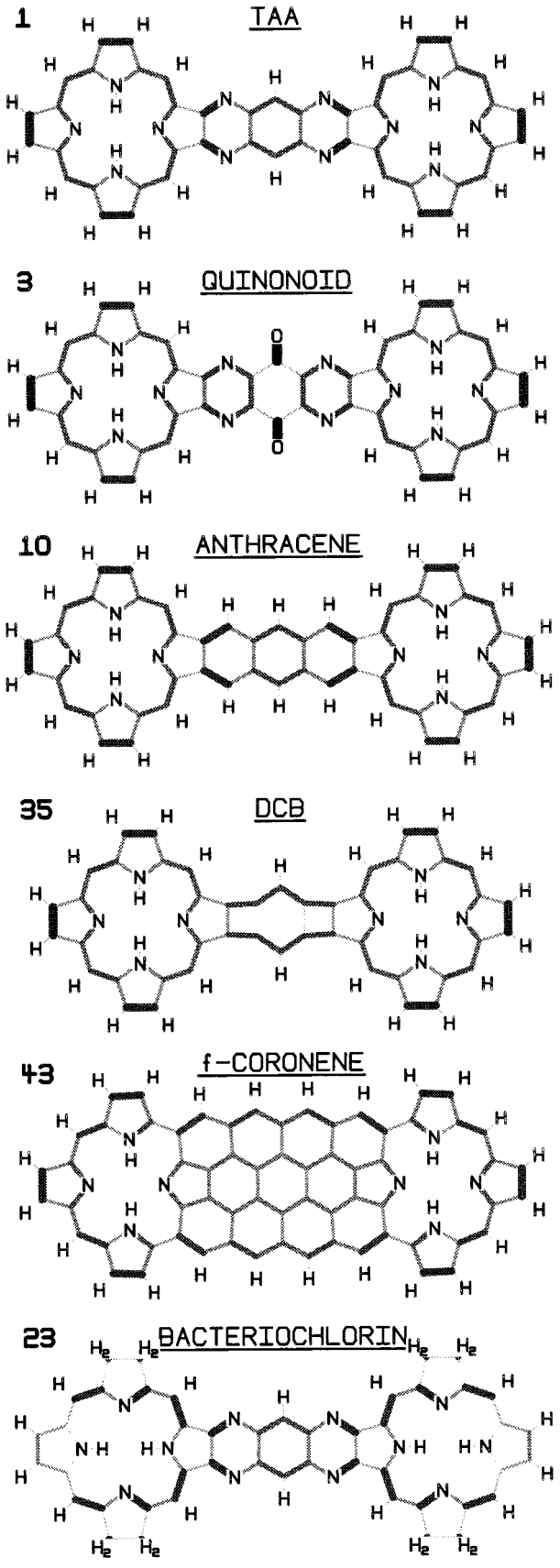


**Figure 6.** Calculated SCF/3-21G atomic bond orders at B3LYP/3-21G geometries for the $P_2B_1$ molecules, top down: **1** (B = TAA); **3** (quinonoid form of **1**); **10** (B = anthracene); **35** (B = DCB); **43** (B = *f*-coronene); **23** (*B* = TAA, bacteriochlorin formed by setting the porphyrin $\beta$ substituent = 2H). Full $\pi$ bonds are indicated by thick black lines, while weak $\pi$ bonds are depicted by thin, faint lines.

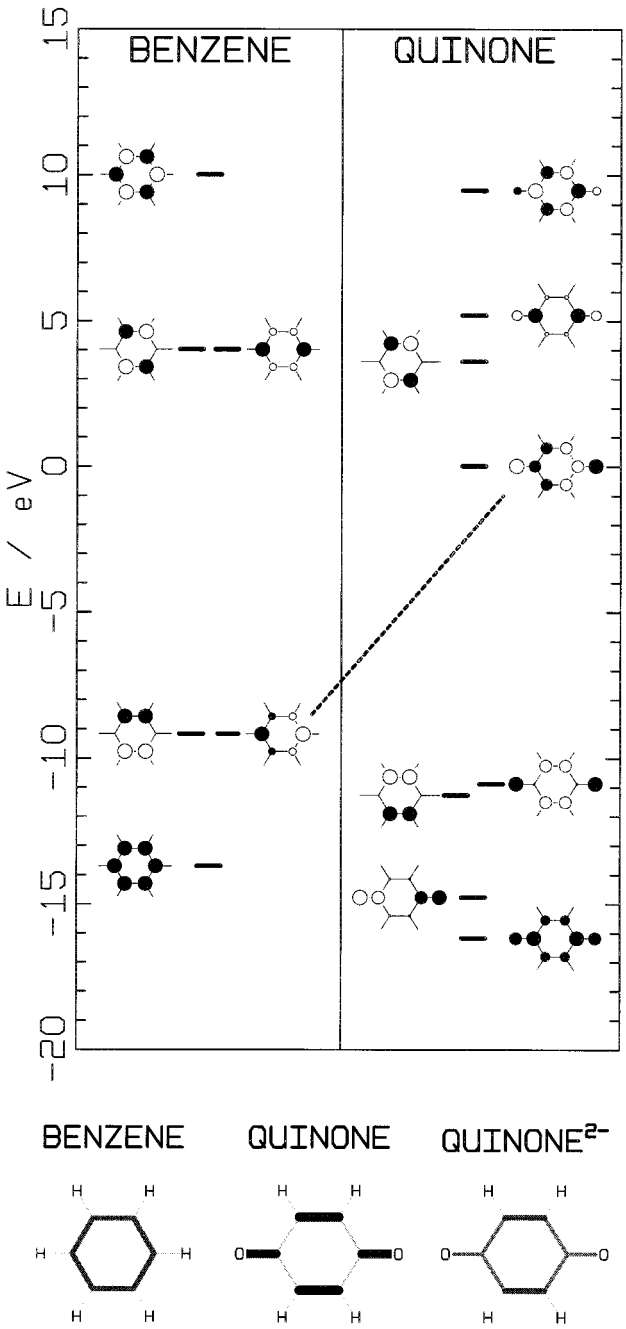


**Figure 7.** Calculated SCF/3-21G wave functions and $\pi$ orbital energies at B3LYP/3-21G geometries for benzene (**69**) and *p*-quinone (**70**). The lower frames show the calculated atomic $\pi$ bond orders for these molecules and that for the dianion *p*-quinone(2−) (at the geometry of the neutral molecule); full $\pi$ bonds are indicated by thick black lines, while weak $\pi$ bonds are depicted by thin, faint lines.

quinonoid switching is expected to be robust and effective for hole-transfer processes, the same is not true for electron-transfer processes with the conductivity predicted to remain high in the quinonoid form. Quantitative calculations also become more difficult as small energy level differences must be faithfully reproduced. Bridge resonances with the SLUMO levels are predicted to occur in bacteriochlorins (**23**−**28**) and for *f*-coronene bridges (**44**), the later offering the best possibilities for exploitation as, for it, the SLUMO levels form the higher-energy unoccupied molecular orbitals.

Almost always the porphyrin LUMO levels interact strongly with bridge levels, and inter-porphyrin couplings are typically within the range 150 meV < $|J|$ < 300 meV. Very little

**TABLE 3: Average Couplings *J* Calculated for Benzenoid $P_2B_1$ Dimers and the Average Attenuation in the Coupling on Conversion from the Benzenoid to Quinonoid Forms[a]**

| interacting porphyrin orbitals | av $\|J\|$ for benzenoid form/meV | av ratio of $\|J\|$ benzenoid:quinonoid |
|---|---|---|
| SLUMO | 180 | 3 |
| LUMO | 200 | 1.4 |
| HOMO | 130 | 15 |
| SHOMO | 17 | 4 |

[a] The averages are for the 12 benzenoid/quinonoid pairs shown in Table 2.

attenuation is predicted after quinonoid conversion, with the coupling strengths often *increasing* slightly. This is a resonance effect, and its origins are depicted in Figure 7 where the $\pi$ SCF/3-21G orbital energies and wave functions at B3LYP/3-21G geometries are reported for benzene (**69**) and *p*-quinone (**70**). Quinonoid conversion pushes occupied bridge orbitals to lower energy, away from porphyrin HOMO and SHOMO orbitals so that inter-porphyrin coupling is reduced. However, one previously occupied bridge orbital is pushed into the HOMO−LUMO gap and becomes unoccupied. This new virtual orbital is at much lower energy than the benzenoid virtual orbitals and falls into resonance with the porphyrin LUMO orbitals, thus *increasing* the coupling. Indeed, it is precisely this orbital (or its anthracene, etc., analogues) which provides the strongest inter-HOMO interaction in the benzonoid oligoporphyrins (see Figure 5). Further, it is the failure of this orbital to be occupied which destroys the $\pi$-electron delocalization through the ring, as exemplified by the largely delocalized pattern shown in Figure 7 for the dianion *p*-quinone(2−) (evaluated at the geometry of the neutral molecule).

While Figure 7 describes the quinonoid switching effect using SCF orbitals, the results are robust and also appear at both CNDO/S and Hückel levels of theory. Suitable Hückel parameters (fitted to CNDO/S Fock matrix elements) are $\alpha_O = \alpha_C + \beta_{CC}$ and $\beta_{CO} = 1.6\ \beta_{CC}$, the first equation incidently resulting in the prediction that the third and fourth *p*-quinone levels are degenerate.

In summary, we see that while simple arguments which link the effectiveness of bridges in providing electronic coupling to the localized/delocalized nature of their $\pi$ bonds are often highly useful, the actual situation for any given system is controlled by the specific nature of resonances within it. In the absence of specific orbital resonance effects (e.g., for the SHOMO and SLUMO orbitals), quinonoid conversion reduces the inter-porphyrin coupling by a factor of 4. This is readily understood in terms of changes to the bridge $\pi$-electron localization. However, when quinonoid conversion removes a key specific orbital interaction (e.g., for the HOMO orbitals), the attenuation is much greater, but when conversions creates a new specific interaction (e.g., for the LUMO orbitals), the attenuation is much less.

Finally, we investigate the effects of chelating Mg, Zn, and $Ru(CO)_2$ within the porphyrin rings. This is usually seen to have only a small effect on the couplings between the porphyrin levels, the most notable being an increase in the SLUMO couplings. For the Ru(II) complexes, one would expect the highest-occupied molecular orbitals to be the three ruthenium $d_{t_{2g}}$ orbitals (with $d_\pi$ the highest). This would have a significant impact for hole transport through these complexes. Our calculations are for gas-phase complexes and do not include the solvation effects which are essential for the correct placement of the ruthenium orbitals, and so they cannot address this issue. We consider it in detail elsewhere, however.[2]

**TABLE 4: Calculated Couplings between the Bridge SHOMO, HOMO, LUMO, and SLUMO Levels in Substituted Symmetrical Dimers $P_1B_2$[a]**

| no. | porphyrin $\beta$ substituent | bridge type | coupling/meV SHOMO | HOMO | LUMO | SLUMO |
|---|---|---|---|---|---|---|
| **45** | H | TAA | −24 | 172 | −140 | 381 |
| **46** | H | anthracene | −15 | 260 | −72 | 477 |
| **47** | 2H | TAA | −52 | 164 | 271 | 226 |
| **48** | 2H[b] | TAA | −40 | 128 | 79 | 135 |
| **49** | 2H[b] | anthracene | −21 | 177 | 94 | 162 |
| **50** | H | DCB | −7 | −386 | −134 | 831 |
| **51** | H | *f*-coronene | 56 | 194 | −347 | −202 |

[a] All molecules have free-base porphyrins (H inner ring) and unsubstituted bridges. TAA, 1,4,5,8,tetraazaanthracene; DCB, dicyclobuta[*a*,*d*]benzene; *f*-coronene, coronene with extra CH's to fuse additional rings to the porphyrin meso positions (see Figure 2). [b] Higher-energy form with the inner hydrogens along the short axis.

**4.2. Variations i and iv of $P_1B_2$.** For oligoporphyrins containing bridges such as acenes, the highest-lying molecular orbitals are porphyrin-like in nature and are thus likely to form the most-important orbitals in electron-transfer applications. However, for bridges containing cyclobutadiene rings and for *f*-coronene, the highest-lying molecular orbitals are bridge orbitals. Here, we consider $P_1B_2$ and investigate the couplings between localized *bridge* SHOMO, HOMO, LUMO, and SLUMO orbitals as mitigated through a central porphyrin. Even if the bridge orbitals do not dominate the frontier molecular orbitals, experimental manifestations of this coupling could be realized by e.g. photoelectron or electronic absorption spectroscopy. Results are given in Table 4 while the bridge-centered molecular orbitals for the basic B = TAA system **45** are shown in Figure 8.

The results obtained are somewhat similar to those obtained for inter-porphyrin coupling in $P_2B_1$ in that replacement of TAA by anthracene increases the coupling of the strongly interacting levels by about 50%. Naively, the inferior coupling of the aza derivative occurs as delocalization is reduced through the azine-containing rings. Similarly, as the internal conjugation is reduced in bacteriochlorin (see Figure 6), so is the through-porphyrin coupling. Resonances abound for the SLUMO levels, making the coupling between them quite strong. The strongest interactions occur between DCB bridges, the ones for which the porphyrin levels most closely match.

**4.3. Protonation of the Azine Nitrogen Atoms of TAA Bridges.** Chemical control of oligoporphyrins bridged by 1,4,5,8-tetraazaanthracene units could very easily be exercised through pH control. Under acidic conditions, one or more protons could be added to the (basic) azine nitrogen atoms, greatly perturbing the electronic structure of the molecule. B3LYP/3-21G optimized gas-phase structures for the singly protonated oligoporphyrin **52** and the *opp* ($C_{2v}$) **53**, syn ($C_{2h}$) **55**, and *anti* ($C_{2v}$) **54** tautomers of the doubly protonated oligoporphyrin have been obtained, and calculated SCF/3-21G orbital properties and atomic $\pi$ bond orders are shown in Table 5 and Figure 9, respectively. Asymmetric protonation as in **52** and **53** induces a large energy shift $e_0$ of order 1.1 eV per proton between the energies of the localized porphyrin levels at each end of the molecule. The inter-porphyrin coupling is not significantly modified, however, and so $e_0$ is calculated to be 1 order of magnitude large than *J*; see Table 5. As a result, asymmetric protonation effectively isolates the two ends of the molecule: using perturbation theory, the fraction of the wave function at one end mixed into the wave function at the other end becomes $J/e_0$ which is very small and so superexchange coupling is heavily damped. Conduction through a protonated

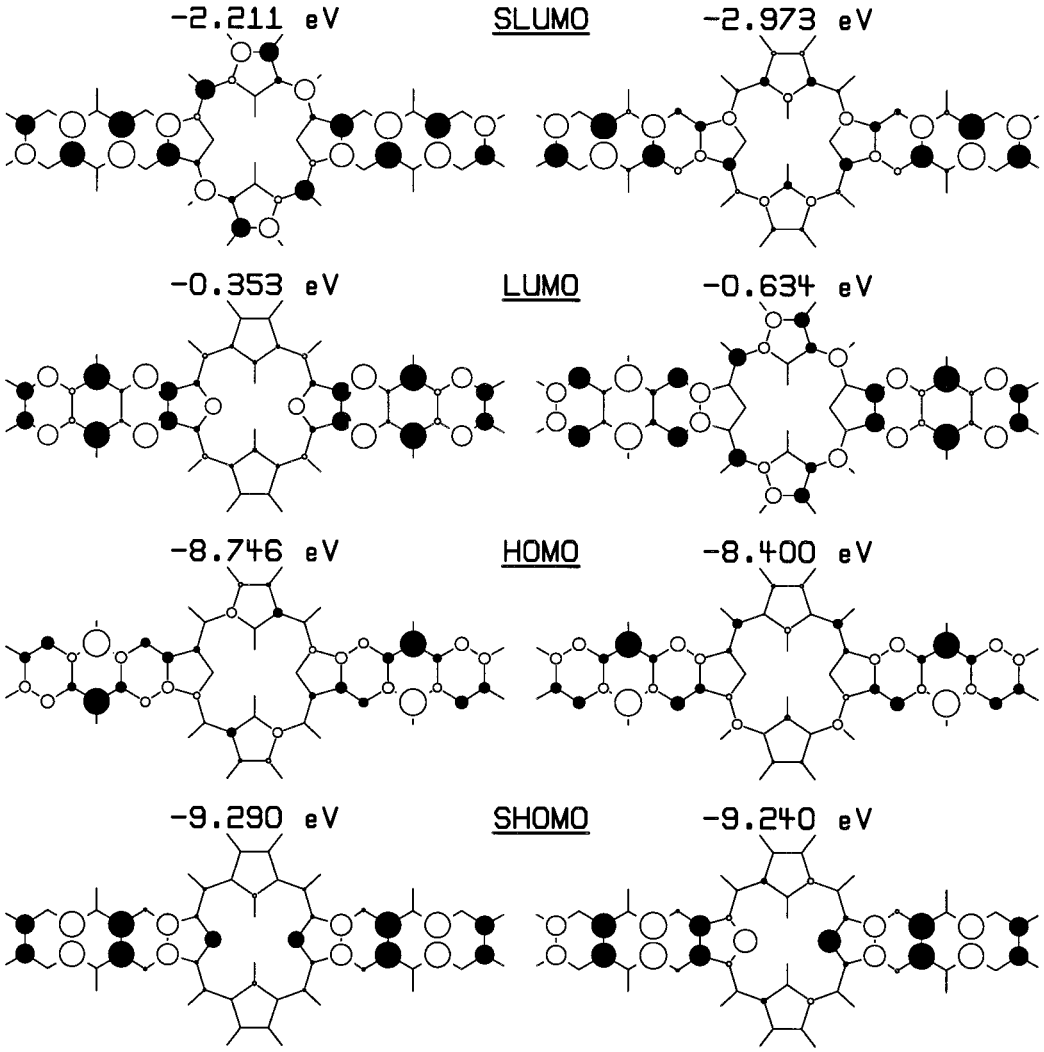


**Figure 8.** Four highest-lying bridge-based occupied molecular orbitals and the lowest-lying unoccupied bridge-based molecular orbitals and their energies for $P_1B_2$ **45** (evaluated SCF/3-21G at the B3LYP/3-21G geometry) analyzed in terms of pairs of localized bridge SHOMO, HOMO, LUMO, and SLUMO levels. The areas of the circles indicate the contribution of the orbital, if occupied, to the atomic Mulliken charge, while open and closed circles are used to indicate the sign of the wave function.

**TABLE 5: $P_2B_1$ with Unsubstituted Free-Base Porphyrin and 1,4,5,8-Tetraazaanthracene Bridge, Protonated at One or Two of the Bridge Nitrogens**

| no. | no. of protons | symmetry | $e_0$/eV | $J$/eV | $\Delta E$/kcal mol$^{-1}$ |
|---|---|---|---|---|---|
| **52** | 1 | $C_s$ | 1.2 | ? | |
| **53** | 2, *opp* | $C_{2v}$ | 2.1 | ? | 16.4 |
| **54** | 2, *anti* | $C_{2h}$ | 0 | 0.123 | 0.2 |
| **55** | 2, *syn* | $C_{2v}$ | 0 | −0.039 | 0 |

[a] $e_0$ is the SCF/3-21G energy difference between the localized HOMO orbitals on each porphyrin; $J$ is the inter-HOMO coupling, and $\Delta E$ is the relative gas-phase energy.

oligoporphyrin wire by means other than superexchange (e.g., polaron or soliton transport) would see this as an impurity site. It could be that protonation acts like a dopant and enhances conductivity through these mechanisms, but such an effect is beyond the scope of this work. Monoprotonation is by necessity asymmetric, and so this effect will always be operative. However, according to the (gas-phase) relative B3LYP/3-21G energies $\Delta E$ shown in Table 5, symmetric bisprotonation (in actually either the *syn* or *anti* form) is much more likely than is asymmetric bisprotonation (in the *opp* form). Hence the major effect of bisprotonation is actually expected to provide variation of the interporphyrin coupling $J$.

### 5. Length Dependence of the End to End Coupling in Linear Oligoporphyrins $P_nB_{n-1}$

For a variety of linear $P_nB_{n-1}$ oligoporphyrins with $n = 2-4$ we have either optimized the geometry using B3LYP or applied the scheme described in section 3 to estimate geometries; see Table 7. As $n$ increases, localized porphyrin and bridge energy levels spread to form (possibly overlapping) bands each containing either $n$ porphyrin or $n - 1$ bridges levels. For the developing porphyrin SHOMO, HOMO, LUMO, and SLUMO bands we express the calculated energy levels in terms of the eigenvalues of the terminally modified Hückel Hamiltonian

$$H = \begin{bmatrix} E+e_0 & J & & \dots & & & & \\ J & E & J & \dots & & & & \\ & J & E & J & \dots & & & \\ \vdots & \vdots & \vdots & \vdots & & \vdots & \vdots & \vdots & \vdots \\ & & & \dots & J & E & J & \\ & & & \dots & & J & E & J \\ & & & \dots & & & J & E+e_0 \end{bmatrix} \quad (1)$$

where $E$ is the energy of an internal-porphyrin localized orbital, $e_0$ is the relative energy of the terminal porphyrin localized orbitals, and $J$ is the inter-porphyrin coupling. The three

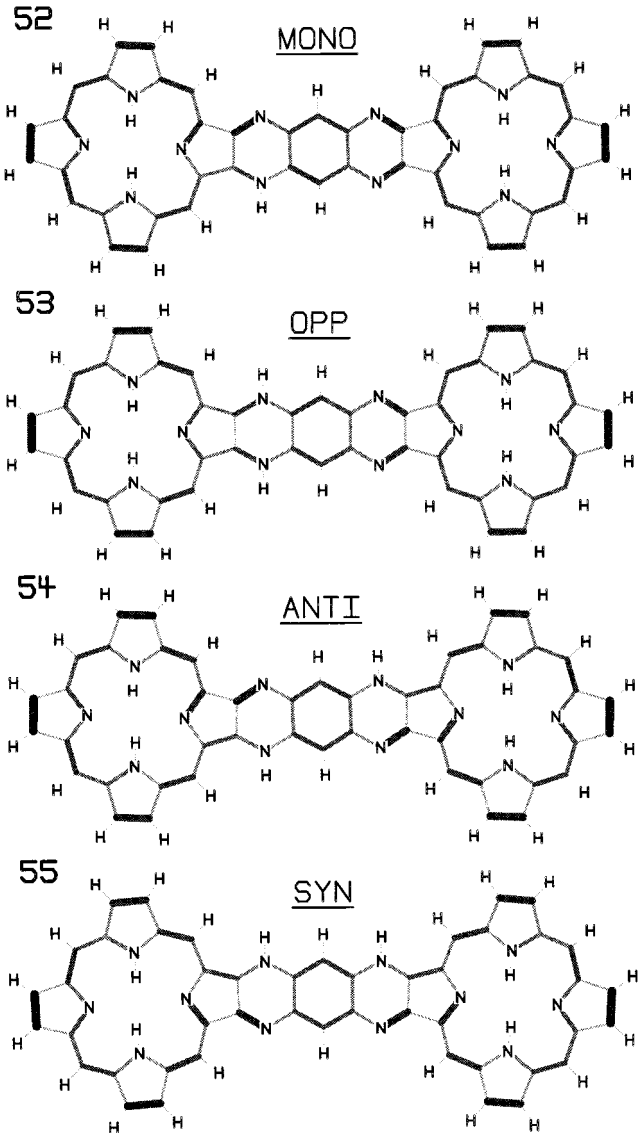


**Figure 9.** Calculated SCF/3-21G atomic bond orders at B3LYP/3-21G geometries for mono protonated and *opp*, *anti*, and *syn* bisprotonated $P_2B_1$ molecules **52**−**55** with B = TAA. Full $\pi$ bonds are indicated by thick black lines, while weak $\pi$ bonds are depicted by thin, faint lines.

parameters $E$, $e_0$, and $J$ are then fitted to the nine SCF-calculated molecular orbital band energies obtained from molecules with $n = 2-4$, and the determined values of $e_0$ and $J$ as well as the root-mean-square errors in this fit are given in Table 7.

In general, the errors in the fits are less than 5% of the range in the data, indicating that the modified Hückel model is appropriate and that the effects of resonances are controlled. The errors are significantly larger for B = DCB, however, and very large for B = *f*-coronene bridges, bridges which do form strong resonance interactions with the porphyrin levels. In these cases to model the energy-level pattern more accurately the Hamiltonian must be expanded to include the appropriate number of resonant bridge states. Nevertheless, the deduced couplings usually agree well with the corresponding ones shown in Table 2 evaluated from just $P_2B_1$ alone, indicating that eq 1 does qualitatively describe the interactions within each molecule. Note, however, that we also performed calculations for the analogous $Ru(CO)_2$-substituted oligoporphyrins (extensions of **44**). Results are not shown in Table 7 as, for $n > 2$, porphyrin-type orbitals could not be identified. This arises because for this bridge it is the porphyrin SHOMO orbitals which very strongly interact, orbitals which have large coefficients on the pyrrole nitrogen atoms and hence interact strongly with coordinated metals. Apparently, this additional interaction is sufficient to destroy the remaining porphyrin-like nature of the orbitals. A consequence of this is that very strong, weakly distance dependent, coupling is predicated to occur between the metal centers.[2]

**TABLE 6: Additional Molecules Optimized with B3LYP/3-21G[a]**

| | | porphyrin | | bridge | |
|---|---|---|---|---|---|
| no. | class | $\beta$ substituent | inner ring | type | substituent |
| **56** | $B_1E_2$[b] | | | benzene | H |
| **57** | $B_1E_2$[b] | | | benzene | O |
| **58** | $P_1B_1$ | H | 2H | TAA | H |
| **59** | $P_1B_2$[c] | H | 2H | TAA | H |
| **60** | $P_1B_3$ | H | 2H | TAA | H |
| **61** | $P_1B_4$ | H | 2H | TAA | H |
| **62** | $P_1B_1$ | H | 2H | TAA | O |
| **63** | $P_1B_1$ | H | $Ru(CO)_2$ | TAA | H |
| **64** | $P_1B_1$ | H | 2H | *f*-anthracene | |
| **65** | $P_1B_1$ | H | 2H | *f*-coronene | |
| **66** | $P_1B_2$ | H | 2H | TAA | O |
| **67** | $B_1E_1$ | | | TAA | H |
| **68** | $B_1E_2$ | | | TAA | O |
| **69** | $B_1$ | | | benzene | H |
| **70** | $B_1$ | | | benzene | O |
| **71** | $B_1$ | | | naphthalene | H |
| **72** | $B_1$ | | | TAA | H |
| **73** | $B_1$ | | | anthracene | H |
| **74** | $B_1$ | | | TAA | O |
| **75** | $B_1$ | | | tetracene | H |
| **76** | $B_1$ | | | DCB | H |
| **77** | $B_1$ | | | biphenylene | H |
| **78** | $B_1$ | | | DCN | H |
| **79** | $B_1$ | | | DCP | H |
| **80** | $B_1$ | | | pyrene | H |
| **81** | $B_1$ | | | coronene | H |
| **82** | $E_1$ | | | | |
| **83** | $E_1$[b] | | | | |
| **84** | $P_1$ | 2H | 2H | | |
| **85** | $P_1$ | H | 2H | | |

[a] TAA, 1,4,5,8-tetraazaanthracene; DCB, dicyclobuta[*a*,*d*]benzene; DCN, dicyclobuta[*b*,*g*]naphthalene; DCP, dicyclobuta[*b*,*h*]biphenylene; *f*-anthracene and *f*-coronene, anthracene and coronene with extra CH's to fuse additional rings to the porphyrin meso positions, respectively (see Figure 2); E, phenanthroline−$[CuCl_2]^-$ except for those with footnote *b*. [b] E is 2-thienyl. [c] Bridge molecules arranged perpendicular ($C_s$ symmetry). **56** is 1,3-bis(2-thienyl)benzene, **57** is 2,6-bis(2-thienyl)-1,4-benzoquinone, **70** is *p*-quinone, **83** is thiophene, **84** is bacteriochlorin, and **85** is free-base porphyrin.

For most bands of most molecules the energy offset for the terminal porphyrins exceeds the energy from the band center to the band edge of an infinite band, $2|J|$ so that the end levels decouple from the inner levels, producing[34] steep McConnell-like[36] exponential decay of the end-to-end coupling with increasing bridge length $n$. When this is not the case, the terminal porphyrins remain resonant with the central ones and rapid end-to-end electron transport is possible provided that the energy levels of the electron or hole sources and sinks are within the band or at most of order $|J|$ away from it (this is true for both molecular[34] and electrode[3−9] connections). For B = TAA, both electron and hole conduction processes could be viable, but the moderate values (ca. 100−200 meV) of $|J|$ necessitate that the relative source/oligoporphyrin/sink potentials be tightly controlled. This could be achieved in laboratory situations, and these molecules do offer the possibility of long-range through-molecule conduction realized over significantly greater distances than has currently been achieved.[3−9] Unfortunately, control of voltages to this order is unlikely in a robust, commercially

**TABLE 7: Fitted Hückel Parameters $e_0$ and $J$ and the Root-Mean-Square Errors in the Fits for the Localized-Porphyrin SHOMO, HOMO, LUMO, and SLUMO Subbands of Oligoporphyrins $P_nB_{n-1}$ over the Range $n = 2-4$[a]**

| | | bridge | | SHOMO/meV | | | HOMO /meV | | | LUMO/meV | | | SLUMO/meV | | |
|---|---|---|---|---|---|---|---|---|---|---|---|---|---|---|---|
| no. | inner ring | type | subst | $e_0$ | $J$ | err | $e_0$ | $J$ | err | $e_0$ | $J$ | err | $e_0$ | $J$ | err |
| 1, 7 | 2H | TAA | H | 190 | −2 | 9 | −8 | 120 | 5 | 90 | 150[b] | 13 | 310 | −100 | 26 |
| 3 | 2H | TAA | O | 250 | −0.3 | 13 | 190 | −6 | 13 | 310 | −170 | 31 | 340 | −28 | 13 |
| 4 | $Ru(CO)_2$ | TAA | H | 110 | −10 | 6 | −40 | 120 | 4 | 300 | 170[b] | 12 | 250 | −150 | 44 |
| 22 | $Ru(CO)_2$ | TAA | O | 210 | −2 | 13 | 230 | −6 | 13 | 450 | −190 | 67 | 350 | −33 | 15 |
| 35, 7 | 2H | DCB | H | 320 | 7 | 19 | 450 | 350[d] | 56 | 340 | −680 | 8 | 350 | 180 | 57 |
| 36 | $Ru(CO)_2$ | DCB | H | 170 | 43 | 25 | 420 | 340[d] | 51 | 360 | −670 | 46 | 110 | 210 | 59 |
| 43, 9 | 2H | *f*-coronene | | 340 | 492 | 160 | 420 | −30[d] | 250 | 680 | 330[c] | 280 | −400 | 350 | 330 |

[a] The numbers of the individually optimized molecules for $n = 2$ and, when available, $n = 3$ (the remaining $n = 3$ molecular geometries and all $n = 4$ molecular geometries are estimated using the technique described in section **3** and Figure 4). TAA, 1,4,5,8-tetraazaanthracene; DCB, dicyclobuta[*a*,*d*]benzene; *f*-coronene, coronene with extra CH's to fuse additional rings to the porphyrin meso positions, respectively (see Figure 2). [b] The SLUMO band is the lowest-energy unoccupied band. [c] A bridge band is the lowest-energy unoccupied band. [d] A bridge band is the highest-energy occupied band.

practical, molecular electronic device. From the results in Table 2 it is clear that, by chemical substitution effects or by replacing TAA with unsubstituted acene bridges, it is possible to increase $|J|$ ]by a factor of 2, but this is not likely to be adequate. Substantial improvements only appear possible when bridges such as DCB and *f*-coronene are used in which bridge levels become resonant with porphyrin levels. In these cases, source/sink energy levels need be controlled only to within the much larger porphyrin-bridge interfragment coupling strength, suggesting that device tolerances could be of order 1 V or larger.

## 6. Conclusions

Oligoporphyrins have many natural advantages as molecular wires in nanoelectronic devices including synthesizability, stability, synthetic flexibility, solubility, rigidity, self-assembly (e.g., on gold surfaces[37] and in Langmuir−Blodgett films[38]), scanning tunneling microscope assembly (e.g., refs 39 and 40), attachment (e.g., by phenanthroline end groups[12]), form junctions, wire functionality, rectification (this functionality is yet to be demonstrated, but appropriate compounds have been synthesized[41]), and switch functionality.[13,16] In the wider picture, we explore the implication of this elsewhere.[2] Here, we have explored the wire functionality in detail, examining how the synthetic flexibility may be exploited in order to optimize results, and the switch functionality, through quinonoid switching of through-bridge coupling.

Investigations of the coupling between porphyrin and bridge $\pi$ levels strongly suggest that, if readily available oligoporphyrin trimers and tetramers are used to bridge nanoelectrodes or STM tips, measurable conductivity[3−9] should result. Further, by designing bridges whose energy levels are resonant with porphyrin levels, we show that it is, in principle, possible to significantly increase the coupling to levels sufficient to provide acceptable tolerance margins in practicable devices. Some of the bridge molecules suggested, principally *f*-coronene (see Figure 2), have energy-level structures so distorted that they are barely recognizable as oligoporphyrins. In fact, they more closely resemble functionalized graphite fragments, and if appropriate synthetic strategies can be developed, materials of this type may become important in molecular electronic applications.

The molecules considered which contain either chelated ruthenium complexes or copper complexes attached to phenanthroline end groups open up possibilities of conduction not just between porphyrin or bridge $\pi$ orbitals but also between metal $d_\pi$ orbitals. Due to the technically more difficult nature of this problem,[30] it is investigated separately.[2] The techniques applied therein have also been applied to investigate intermetallic coupling[42] through the bis(pentaammineruthenium) complexes of the $\alpha,\omega$-dipyridyl *trans*-polyenes synthesized by Woitellier, Launay, and Spangler.[43]

Throughout we have considered superexchange coupling using effective two-level models. While it is straightforward to extend this treatment to avoid effective two-level models and thus improve quantitative accuracy,[2,33] treatment of conductivity mechanisms other than superexchange such as polaron or soliton transport a priori is very much more difficult (consider e.g. treatments of soliton transport through polyacetylene fragments[44]). Superexchange couplings through oligoporphyrins are sufficiently weak that localized charge transfer processes along chains would readily become the dominant mechanism. However, interunit couplings which control the superexchange also control rates of localized charge-transfer processes and so the principles extracted here are expected to be of general importance.

Finally, we note that, in addition to switching conductivity, quinonoid conversion also results in significant color switching. The reason for this is apparent in Figure 7 which shows that the quinonoid form has an unoccupied molecular orbital located within the band gap of the benzenoid form; this gives rise to an intense quinonoid band which, for conjugated bridges, occurs in the visible region. While this band is overshadowed by the extremely intense porphyrin transitions in oligoporphyrins, in non-porphyrin systems the color change could be profound, e.g., quinacridone pigments are brightly colored quinonoid molecules while their corresponding benzenoid forms are colorless. Possible hydrogen-tautomerization-based solid-state quinonoid color switching devices are also discussed in detail elsewhere.[16] In oligoporphyrins,[13] the major influence which this quinone orbital has on absorption spectra is the appearance of a moderately strong porphyrin to quinone charge-transfer band at ca. 480 nm.

**Acknowledgment.** Support from the Australian Research Council for this project is gratefully acknowledged.

**Supporting Information Available:** Tables and figures containing the B3LYP/3-21G structures, optimized geometries, and Mulliken charges for molecules **1**−**85** described in Tables 1, 2, 4, and 5. This material is available free of charge via the Internet at http:/pubs.acs.org.

## References and Notes

(1) Crossley, M. J.; Burn, P. L. *J. Chem. Soc., Chem. Commun.* **1991**, 1569.

(2) Hush, N. S.; Reimers, J. R.; Hall, L. E.; Johnston, L. A.; Crossley, M. J. *Ann. N. Y. Acad. Sci.* **1998**, *852*, 1.

(3) Mujica, V.; Kemp, M.; Roitberg, A.; Ratner, M. A. *J. Chem. Phys.* **1996**, *104*, 7296.
(4) Bumm, L. A.; Arnold, J. J.; Cygan, M. T.; Dunbar, T. D.; Burgin, T. P.; Jones, L., II; Allara, D. L.; Tour, J. M.; Weiss, P. S. *Science* **1996**, *271*, 1705.
(5) Reed, M. A.; Zhou, C.; Muller, C. J.; Burgin, T. P.; Tour, J. M. *Science* **1997**, *278*, 252.
(6) Datta, S.; Tian, W.; Kubiak, C. P. *Proc. Electrochem. Soc.* **1997**, *97*, 211.
(7) Datta, S.; Tian, W.; Hong, S.; Reifenberger, R.; Henderson, J. I.; Kubiak, C. P. *Phys. Rev. Lett.* **1997**, *79*, 2530.
(8) Roth, S.; Joachim, C. *Atomic and molecular wires*; Kulwer: Dordrecht, The Netherlands, 1997.
(9) Ratner, M. A.; Davis, B.; Kemp, M.; Mujica, V.; Roitberg, A.; Yaliraki, S. *Ann. N. Y. Acad. Sci.* **1998**, *852*, 22.
(10) Crossley, M. J.; Burn, P. L. *J. Chem. Soc., Chem. Commun.* **1987**, 39.
(11) Crossley, M. J.; Govenlock, L. J.; Prashar, J. K. *J. Chem. Soc., Chem. Commun.* **1995**, 2379.
(12) Crossley, M. J.; Burn, P. L.; Langford, S. J.; Prashar, J. K. *J. Chem. Soc., Chem. Commun.* **1995**, 1921.
(13) Crossley, M. J.; Johnston, L. A.; Reimers, J. R.; Hush, N. S. *J. Am. Chem. Soc.*, in preparation.
(14) Crossley, M. J.; Prashar, J. K. *Tetrahedron Lett.* **1997**, *38*, 6751.
(15) Lü, T. X.; Reimers, J. R.; Crossley, M. J.; Hush, N. S. *J. Phys. Chem.* **1994**, *98*, 11878.
(16) Reimers, J. R.; Hall, L. E.; Hush, N. S.; Silverbrook, K. *Ann. N. Y. Acad. Sci.* **1998**, *852*, 38.
(17) Reimers, J. R.; Lü, T. X.; Crossley, M. J.; Hush, N. S. *J. Am. Chem. Soc.* **1995**, *117*, 2855.
(18) Almlöf, J.; Fischer, T. H.; Gassman, P. G.; Ghosh, A.; Häser, M. *J. Phys. Chem.* **1993**, *97*, 10964.
(19) Merchán, M.; Ortí, E.; Roos, B. O. *Chem. Phys. Lett.* **1994**, *221*, 136.
(20) Frisch, M. J.; Trucks, G. W.; Schlegel, H. B.; Gill, P. M. W.; Johnson, B. G.; Robb, M. A.; Cheeseman, J. R.; Kieth, T. A.; Petersson, G. A.; Montgomery, J. A.; Raghavachari, K.; Al-Laham, M. A.; Zakrzewski, V. G.; Ortiz, J. V.; Foresman, J. B.; Cioslowski, J.; Stefanov, B. B.; Nanayakkara, A.; Challacombe, M.; Peng, C. Y.; Ayala, P. A.; Chen, W.; Wong, M. W.; Andres, J. L.; Replogle, E. S.; Gomperts, R.; Martin, R. L.; Fox, D. J.; Binkley, J. S.; DeFrees, D. J.; Baker, J.; Stewart, J. J. P.; Head-Gordon, M.; Gonzalez, C.; Pople, J. A. *GAUSSIAN 94*; Gaussian Inc.: Pittsburgh, PA, 1995.
(21) Ghosh, A.; Gassman, P. G.; Almlöf, J. *J. Am. Chem. Soc.* **1992**, *114*, 4, 9990.
(22) Ghosh, A.; Gassman, P. G.; Almlöf, J. *J. Am. Chem. Soc.* **1994**, *116*, 1932.
(23) Bauernschmitt, R.; Ahlrichs, R. *J. Chem. Phys.* **1996**, *22*, 9047.
(24) Chen, B. M. L.; Tulinsky, A. *J. Am. Chem. Soc.* **1972**, *94*, 4144.
(25) Kozlowski, P. M.; Jarzęcki, A. A.; Pulay, P. *J. Phys. Chem.* **1996**, *100*, 7007.
(26) Dupuis, P.; Roberge, R.; Sandorfy, C. *Chem. Phys. Lett.* **1980**, *75*, 434.
(27) Ghosh, A. *J. Phys. Chem. B* **1997**, *101*, 3290.
(28) Ashkenazi, J.; Picket, W. E.; Krakauer, H.; Wang, C. S.; Klein, B. M.; Chubb, S. R. *Phys. Rev. Lett.* **1989**, *62*, 2016.
(29) Vogl, P.; Campbell, D. K. *Phys. Rev.* **1989**, *B41*, 12797.
(30) Reimers, J. R.; Hush, N. S. *J. Phys. Chem. A* **1999**, *103*, 3066.
(31) Ahlrichs, R.; et al. TURBOMOLE-4, Quantum Chemistry Group, University of Karlsruhe.
(32) Bauernschmitt, R.; Ahlrichs, R. *Chem. Phys. Lett.* **1996**, *256*, 454.
(33) Reimers, J. R.; Hush, N. S. *Chem. Phys.* **1989**, *134*, 323.
(34) Reimers, J. R.; Hush, N. S. *J. Photochem. Photobiol. A* **1994**, *82*, 31.
(35) Villar, H. O.; Dupuis, M. *Chem. Phys. Lett.* **1987**, *142*, 59.
(36) McConnell, H. M. *J. Chem. Phys.* **1961**, *35*, 508.
(37) Crossley, M. J.; Martin, A. S.; Johnston, L. A.; Tansey, C. W. *Adv. Mater.*, manuscript in preparation.
(38) Azumi, R.; Mutsuyoshi, M.; Kuroda, S.; King, L. G.; Crossley, M. J. *Langmuir* **1995**, *11*, 4056.
(39) Jung, T. A.; Schlittler, R. R.; Gimzewski, J. K.; Tang, H.; Joachin, C. *Science* **1997**, *271*, 181.
(40) Jung, T. A.; Schlittler, R. R.; Gimzewski, J. K. *Nature* **1996**, *386*, 696.
(41) Crossley, M. J.; Sheehan, C. S. *J. Chem. Soc., Perkin Trans. 1*, submitted for publication.
(42) Reimers, J. R.; Hush, N. S. *Inorg. Chem.* **1990**, *29*, 4510.
(43) Woitellier, S.; Launay, J. P.; Spangler, C. W. *Inorg. Chem.* **1989**, *28*, 758.
(44) Reimers, J. R.; Craw, J. S.; Bacskay, G. B.; Hush, N. S. *Biosystems* **1995**, *35*, 107.